Excitation of the $^3P_{J=0,1,2}$ fine-structure levels of atomic oxygen in collisions with oxygen atoms

B. Zygelman
Department of Physics, University of Nevada at Las Vegas, Las Vegas, Nevada 89154

A. Dalgarno
Harvard Smithsonian Center for Astrophysics, 60 Garden Street, Cambridge, Massachusetts 02138

R. D. Sharma
Optical Environment Division, Phillips Laboratory, 29 Randolph Road, Hanscom Air Force Base, Massachusetts 01731-3010

(Received 31 May 1994)

A fully quantal calculation of the excitation cross sections for the fine-structure levels of ground-state atomic oxygen, in collisions with oxygen atoms at low energies, is presented. The results are compared with the cross sections obtained in a previous calculation.

PACS number(s): 34.10.+x, 34.20.Cf, 34.50.−s

I. INTRODUCTION

Collisions among oxygen atoms, in which excitation and quenching of the fine-structure levels of their ground state occur, play an important role in determining the heat budget of the terrestrial atmosphere [1]. There are three fine-structure levels in the ^3P ground state of an oxygen atom. In its upper, $J=0$, level, the atom has a dominant decay mode into the $J=1$ level with a lifetime of 16.3 h [2]. This transition involves the emission of a 145.5-μm photon and in the $J=1$ fine-structure level the atom decays into the $J=2$ ground level followed by the emission of a 63.2-μm photon. The lifetime of the $J=1$ state is 3.1 h [2]. These far-infrared emissions may serve as a valuable diagnostic for the atomic oxygen density in planetary atmospheres [3], but accurate modeling of the atomic fine-structure populations requires knowledge of the collision cross sections.

In a previous calculation, Allison and Burke reported [4] values of cross sections for an oxygen atom to undergo a fine-structure transition in collisions with oxygen atoms. However, Grossmann and Offermann [5] suggested, based on an analysis of sounding-rocket remote-sensing observations of the 63.2-μm emissions, that Allison and Burke may have overestimated the values for these cross sections by as much as a factor of 10^4.

In a recent paper Zygelman, Dalgarno, and Sharma [6,7] (which we refer to as Paper I below) introduced a molecular theory of the fine-structure excitation of oxygen atoms by collisions with atomic oxygen, which included molecular and spin-orbit effects ignored in the previous calculation [4]. Here, we report the results of our calculations for the fine-structure excitation cross sections of the $J=2,1,0$ levels in collisions of oxygen atoms at energies corresponding to gas temperature in the range $T\approx 680-2000$ K.

In Sec. II we briefly review the scattering formalism introduced in Paper I and applied to the present calculation. In Sec. III we assemble, discuss, and assess the accuracy of available potential curves for the O_2 molecule that are needed in the scattering calculation. In Sec. IV we derive the radial scattering equations in the L-S representation. This representation allows tremendous simplification in the calculation of the scattering amplitudes for the system of coupled equations. However, the L-S approximation is only valid if the spin-orbit interaction, or the fine-structure splitting, can be neglected. This approximation was employed in the calculation of Allison and Burke, but in our discussion we apply the L-S approach as a diagnostic check on the integrity of the more complex scattering code in the j-j coupling scheme. In Sec. V we discuss our results and compare our cross sections with those given in Ref. [4]. We show that the simplifying assumptions used in that calculation greatly overestimate some of the fine-structure transition cross sections. Atomic units are used, unless otherwise stated, throughout the discussion.

II. SCATTERING FORMALISM

In Paper I we introduced a molecular-state close-coupling theory of the collision process

$$O(^3P_{j_a})+O(^3P_{j_b})\rightarrow O(^3P_{j_a'})+O(^3P_{j_b'}) , \tag{1}$$

and since the theory has been described in detail there, we review only the main features of it. The scattering amplitudes that describe process (1) are expanded into a partial-wave sum and the radial amplitudes $G^{JM}_{jlj_aj_b}(R)$, where JM are the total and azimuthal angular-momentum quantum numbers, j is the total electronic angular momentum of the separated atoms [8], l is the orbital angular-momentum quantum number of the nuclear motion, and j_a, j_b are the total electronic angular-momentum quantum numbers for atoms a and b respectively, obey the coupled radial equations [6]

$$-\frac{1}{2\mu}\left[\frac{d^2}{dR^2}-\frac{l(l+1)}{R^2}\right]G^{JM}_{jlj_aj_b}(R)$$
$$+\sum_{j'l'j'_aj'_b} V^{jlj_aj_b}_{j'l'j'_aj'_b}(JM;R)G^{JM}_{j'l'j'_aj'_b}(R)$$
$$=[E-\Delta E_a(j_a)-\Delta E_b(j_b)]G^{JM}_{jlj_aj_b}(R)\ . \quad (2)$$

In Eq. (2), $\Delta E_a(j_a)$ and $\Delta E_b(j_b)$ are the energy defects of the individual fine-structure levels of atoms a and b, respectively, E is the total energy in the center-of-mass frame, μ is the nuclear reduced mass, and $V^{jlj_aj_b}_{j'l'j'_aj'_b}(JM;R)$ is a radial multipole potential. $V^{jlj_aj_b}_{j'l'j'_aj'_b}(JM;R)$ is an $N\times N$ matrix, where N is the number of channels and each channel represents one particular combination, out of a total of 81, of the quantum numbers $\{jlj_aj_b\}$. Each entry in the potential matrix is a linear combination of products involving $3j$ and $9j$ symbols and Born-Oppenheimer potentials $\epsilon_{\Lambda SL}(R)$,

$$V^{jlj_aj_b}_{j'l'j'_aj'_b}(JM;R)=\sum_{\Lambda\Sigma}\sum_{LS}\sum_{\Omega}[j,j',j_a,j'_a,j_b,j'_b,l,l']^{1/2}[L,S]$$
$$\times\begin{pmatrix} j & l & J\\ \Omega & 0 & -\Omega\end{pmatrix}\begin{pmatrix} L & S & j\\ \Lambda & \Sigma & -\Omega\end{pmatrix}\begin{pmatrix} L & S & j'\\ \Lambda & \Sigma & -\Omega\end{pmatrix}\begin{pmatrix} j' & l' & J\\ \Omega & 0 & -\Omega\end{pmatrix}$$
$$\times\begin{Bmatrix} l_a & s_a & j_a\\ l_b & s_b & j_b\\ L & S & j\end{Bmatrix}\begin{Bmatrix} l'_a & s'_a & j'_a\\ l'_b & s'_b & j'_b\\ L & S & j'\end{Bmatrix}\epsilon_{\Lambda SL}(R)\ . \quad (3)$$

In our notation the Born-Oppenheimer potentials $\epsilon_{\Lambda SL}(R)$ are identified by Λ, the quantum number of the electronic orbital angular momentum projected along the internuclear axis, S, the total spin angular momentum, and L, the quantum number associated with the total orbital angular momentum of the electrons in the separated-atom limit [8]. In Eq. (3) we used the shorthand notation

$$[a,b,\ldots,c]\equiv(2a+1)(2b+1)\cdots(2c+1)\ .$$

Table I illustrates the relationships between the atomic and molecular quantum numbers for each of the 18 electronic states of the O_2 molecule that dissociate to ground-state atomic oxygen atoms. Because our formalism takes into account the different fine-structure levels of the separated atoms, we need to consider 81 distinct channels. Potential (3) consists of 81×81 entries and each entry corresponds to a distinct pair $\{jlj_aj_b\},\{j'l'j'_aj'_b\}$. For the partial wave JM [9], and channel $\{jlj_aj_b\}$, we obtain N independent solutions to Eq. (2). We therefore construct an $N\times N$ matrix whose columns are the N solution vectors to Eq. (2),

$$\underline{G}(JM,R)\equiv G^{j'l'j'_aj'_b}_{jlj_aj_b}(JM,R)\ . \quad (4)$$

The superscript, or column index, identifies a particular solution to Eq. (2) and the subscript, or row index, identifies the channel index. We impose standard scattering boundary conditions [6] and construct the symmetric K matrix $\underline{K}(J)$ [6] and the S matrix

$$\underline{S}(J)=\frac{\underline{I}+i\underline{K}(J)}{\underline{I}-i\underline{K}(J)}\ . \quad (5)$$

The cross section for a pair of oxygen atoms initially in fine-structure states j'_a,j'_b to make a transition into levels j_a,j_b is [6]

TABLE I. Connections between atomic and molecular states for two oxygen ^3P atoms.

Molecular state	Atomic state	C_5	C_6
$a\,^1\Delta g$	$\|L=2\Lambda=\pm2S=0\Sigma\rangle$	0.931	17.05
$1\,^1\Pi_g$	$\|L=2\Lambda=\pm1S=0\Sigma\rangle$	−3.73	16.49
$1\,^1\Pi_u$	$\|L=1\Lambda=\pm1S=0\Sigma\rangle$	0.0	16.49
$c\,^1\Sigma^-_u$	$\|L=1\Lambda=0S=0\Sigma\rangle$	0.0	17.10
$b\,^1\Sigma^+_g$	$\|L=0\Lambda=0S=0\Sigma\rangle$	0.0	16.72
$2\,^1\Sigma^+_g$	$\|L=2\Lambda=0S=0\Sigma\rangle$	5.59	16.35
$C\,^3\Delta_u$	$\|L=2\Lambda=\pm2S=1\Sigma\rangle$	0.931	17.05
$1\,^3\Pi_u$	$\|L=2\Lambda=\pm1S=1\Sigma\rangle$	−3.73	16.49
$1\,^3\Pi_g$	$\|L=1\Lambda=\pm1S=1\Sigma\rangle$	0.0	16.49
$X\,^3\Sigma^-_g$	$\|L=1\Lambda=0S=1\Sigma\rangle$	0.0	17.10
$A\,^3\Sigma^+_u$	$\|L=0\Lambda=0S=1\Sigma\rangle$	0.0	16.72
$2\,^3\Sigma^+_u$	$\|L=2\Lambda=0S=1\Sigma\rangle$	5.59	16.35
$^5\Delta_g$	$\|L=2\Lambda=\pm2S=2\Sigma\rangle$	0.931	17.05
$^5\Pi_g$	$\|L=2\Lambda=\pm1S=2\Sigma\rangle$	−3.73	16.49
$1\,^5\Pi_u$	$\|L=1\Lambda=\pm1S=2\Sigma\rangle$	0.0	16.49
$^5\Sigma^-_u$	$\|L=1\Lambda=0S=2\Sigma\rangle$	0.0	17.10
$1\,^5\Sigma^+_g$	$\|L=0\Lambda=0S=2\Sigma\rangle$	0.0	16.72
$2\,^5\Sigma^+_g$	$\|L=2\Lambda=0S=2\Sigma\rangle$	5.59	16.35

$$\sigma(j_a' j_b' \to j_a j_b) = \frac{\pi}{2k^2_{j_a' j_b'}(2j_a'+1)(2j_b'+1)} \times \sum_{j'l'jl} \sum_{J} (2J+1) |\underline{T}^{j'l'j_a'j_b'}_{jlj_a j_b}(J) + (-1)^{j+l+j_a+j_b} \underline{T}^{j'l'j_a'j_b'}_{jlj_b j_a}(J)|^2 , \quad (6)$$

where

$$[\underline{T}(J)]^{j'l'j_a'j_b'}_{jlj_a j_b} = [\underline{I} - \underline{S}(J)]^{j'l'j_a'j_b'}_{jlj_a j_b} , \quad (7)$$

and

$$k_{j_a j_b} \equiv \sqrt{2\mu[E - \Delta E_a(j_a) - \Delta E_b(j_b)]} \quad (8)$$

is the wave number for the system in the incident channel.

In deriving Eq. (6) we took into account the fact that the nuclei of the collision system are identical bosons and that the total wave function of the system must be symmetric under the interchange of the nuclei.

III. MOLECULAR POTENTIALS

Liu and Saxon [10] have calculated, using an *ab initio* theory, and tabulated the potential-energy curves for all 18 states of O_2 that dissociate to oxygen atoms in their ground state. In a more recent calculation, Partridge *et al.* [11] tabulated the potential-energy curves for the eight bound and weakly bound states $c\,^1\Sigma_u^-$, $C\,^3\Delta_u$, $A\,^3\Sigma_u^+$, $^5\Pi_g$, $1\,^3\Pi_u$, $1^1\Pi_g$, $^5\Sigma_u^-$, and $1\,^5\Pi_u$, of the O_2 molecule [12]. The Liu-Saxon calculations employed a first-order configuration-interaction (FOCI) method, but Partridge *et al.* argued that their multireference configuration-interaction treatment including a Davidson correction (MRCI+Q) is more reliable.

In order to construct potential matrix (3) in the molecular region ($R < 10a_0$), we adopt the values for the Born-Oppenheimer potentials calculated by Liu and Saxon, and for the eight states listed above we use the more accurate *ab initio* potentials reported by Partridge *et al.* At internuclear distances $R \approx 10a_0$ we spline-fit the *ab initio* values so that they smoothly merge to the correct asymptotic limits predicted by the leading-order, long-range, atom-atom potential

$$V_{\text{long range}} = \frac{C_5}{R^5} - \frac{C_6}{R^6} . \quad (9)$$

C_5 is a coefficient that measures the strength of the quadrupole-quadrupole interaction between a pair of ground-state oxygen atoms [6,14–16]. C_6 is the van der Waals coefficient and, for a pair of oxygen atoms, it has been tabulated [17] in the form of matrix elements $C_6(M_a M_b; M_a' M_b')$, which depend on the initial, $M_a M_b$, and final, $M_a' M_b'$, magnetic quantum numbers of the separated atoms a and b, respectively. Neglecting the negligible [17] off-diagonal elements of $C_6(M_a M_b; M_a' M_b')$, we get

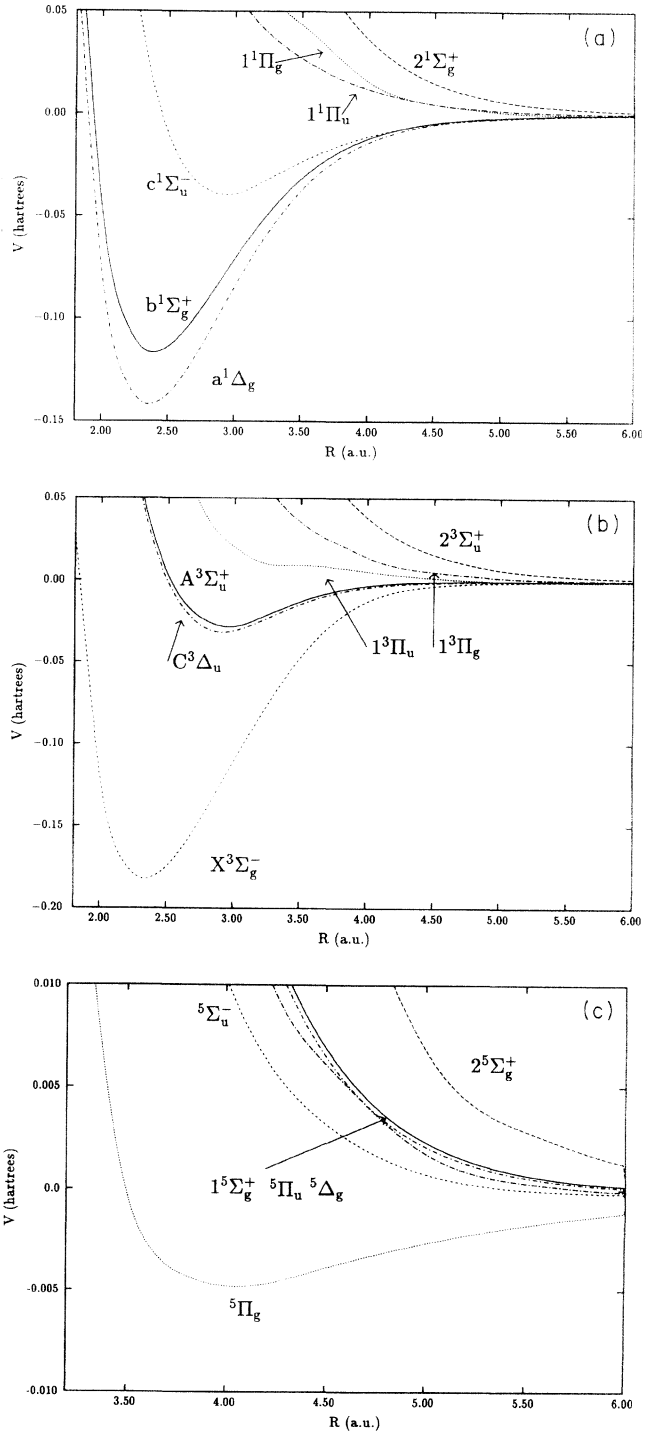

FIG. 1. Potential curves for (a) ground singlet states of O_2, (b) ground triplet states of O_2, and (c) ground quintet states of O_2.

$$C_6(L\Lambda)=\sum_{M_aM_b}(2L+1)\begin{bmatrix}1 & 1 & L\\ M_a & M_b & -\Lambda\end{bmatrix}^2 \times C_6(M_aM_b;M_aM_b)\,, \tag{10}$$

where $C_6(L\Lambda)$ are the van der Waals coefficients that correspond to the diagonal matrix elements of the induced dipole interaction in a representation that is diagonal with respect to the total angular momentum L of the atom-atom system. Using the values given in Ref. [17] we use relation (10) to obtain the $C_6 \equiv C_6(L\Lambda)$ coefficient for each molecular state of the O_2 system considered

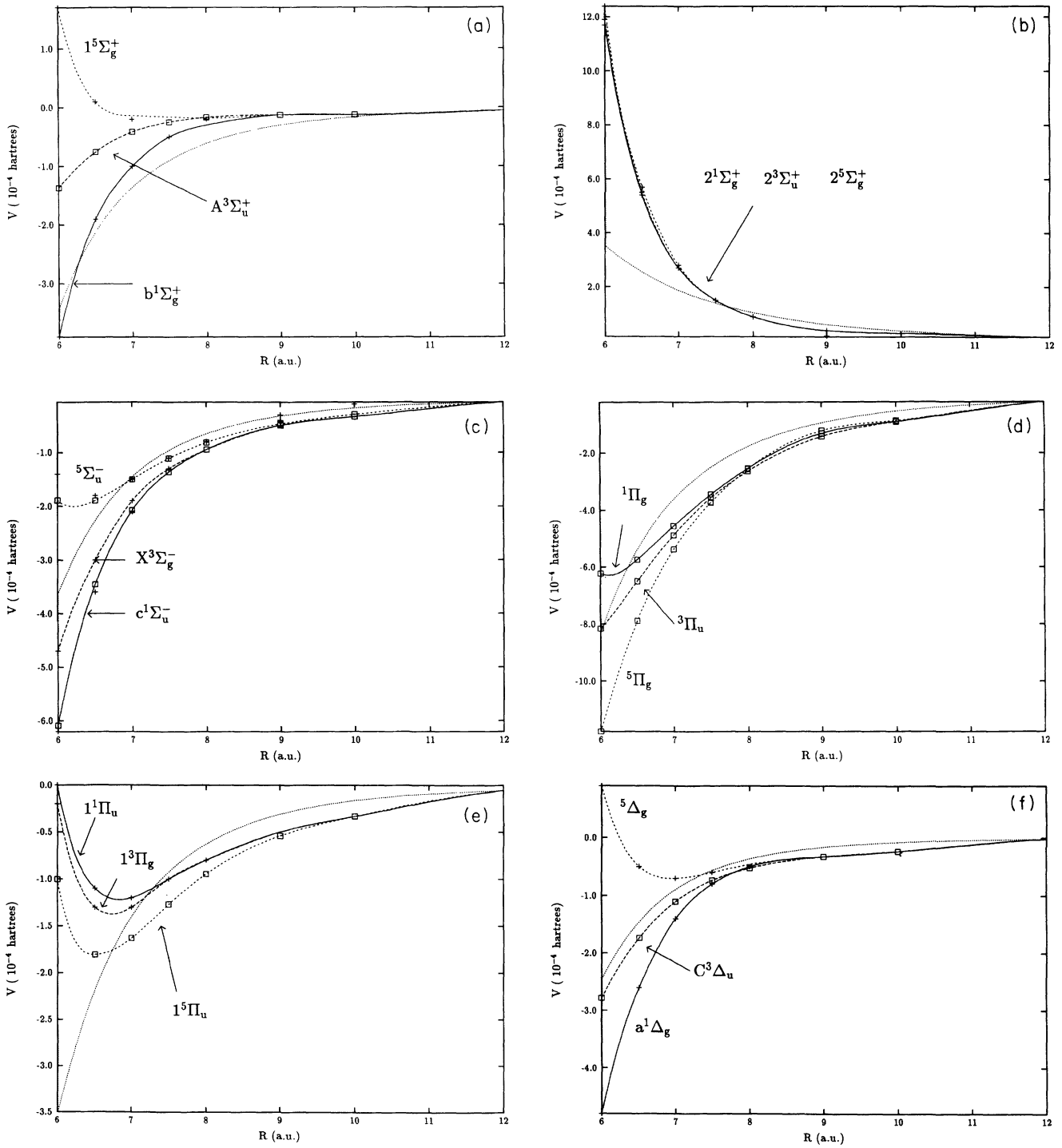

FIG. 2. Potential curves for molecular states correlating to (a) the $L=0$ $M=0$ atomic states, (b) the $L=2$ $M=0$ atomic states, (c) the $L=1$ $M=0$ atomic states, (d) the $L=2$ $M=1$ atomic states, (e) the $L=1$ $M=1$ atomic states, and (f) the $L=2$ $M=2$ atomic states. Dotted lines represent the long-range form given by Eq. (9), boxes represent data from Ref. [11], and crosses denote data from Ref. [10].

here. The numerical values for the C_6 coefficients are tabulated in Table I.

The 18 potential curves used in the present calculation are plotted in Figs. 1(a)–1(c). In Figs. 2(a)–2(f) we plot the six long-range components, each corresponding to atomic states with definite values of L and Λ. In the molecular region, exchange forces split energies (9) into singlet ($S=0$), triplet ($S=1$), and quintet ($S=2$) components. In the region where the molecular description is less reliable, at $R \approx 10a_0$, we ignore small exchange effects and construct the potentials by setting the singlet, triplet, and quintet energies (for a given set L,Λ) to the values obtained by the calculation of Partridge *et al.* [11].

In Fig. 2 we plot the potentials (dashed and solid lines) constructed by us and used in the collision calculations. The dotted lines are the long-range energies (9), the open boxes are the values tabulated by Partridge *et al.* [11], and the crosses are the values tabulated by Liu and Saxon [10].

IV. THE *L-S* REPRESENTATION

In the theory outlined in Ref. [6] the close-coupling expansion was carried out using basis states that diagonalize the spin-orbit interaction of the electrons with the nuclei in the separated-atom limit. These states are identified by the quantum numbers $\{j\Omega j_a j_a\}$ where j, j_a, j_b are defined above and Ω is the projection of j along the internuclear axis. If the spin-orbit-interaction term is neglected, then it is valid to use a representation in which the atomic states are identified by the set of quantum numbers $\{L\Lambda S\Sigma\}$, where L is the total electronic orbital angular momentum, Λ is the projection of the electronic orbital angular momentum on the internuclear axis, S is the total spin, and Σ is the projection of the total spin on the internuclear axis. The two representations are related by a unitary transformation [6],

$$|j\Omega j_a j_b\rangle = \sum_{\Lambda S\Sigma L} W^{j\Omega j_a j_b}_{\Lambda S\Sigma L} |\Lambda S\Sigma L\rangle \ , \tag{11}$$

where

$$W^{j\Omega j_a j_b}_{\Lambda S\Sigma L} = [j, j_a, j_b, L, S]^{1/2} \times (-1)^{j+\Omega} \begin{bmatrix} L & j & S \\ \Lambda & -\Omega & \Sigma \end{bmatrix} \begin{Bmatrix} l_a & s_a & j_a \\ l_b & s_b & j_b \\ L & S & j \end{Bmatrix} ,$$

and (12)

$$\sum_{\Lambda S\Sigma L} W^{j\Omega j_a j_b}_{\Lambda S\Sigma L} W^{j'\Omega' j'_a j'_b}_{\Lambda S\Sigma L} = \delta_{j,j'} \delta_{j_a,j'_a} \delta_{j_b,j'_b} \delta_{\Omega,\Omega'} \ , \tag{13}$$

$$\sum_{j\Omega j_a j_b} W^{j\Omega j_a j_b}_{\Lambda S\Sigma L} W^{j\Omega j_a j_b}_{\Lambda' S'\Sigma' L'} = \delta_{L,L'} \delta_{\Lambda,\Lambda'} \delta_{S,S'} \delta_{\Sigma,\Sigma'} \ .$$

Following the convention in Paper I, $|\Lambda S\Sigma L\rangle$ represents the Born-Oppenheimer molecular eigenfunction whose electronic angular momentum is quantized with respect to the $\hat{z}$ axis of the laboratory frame, and L is an index that identifies the atomic state $|L\Lambda S\Sigma\rangle$ which evolves from it in the separated-atom limit [6]. L is a good quantum number only in the separated-atom limit. The one-to-one mapping of the Born-Oppenheimer states with the atomic states $|L\Lambda S\Sigma\rangle$, is given in Table I. In Paper I we performed a series of unitary, or gauge, transformations on the molecular basis equations to derive the set of radial equations (2). In the following discussion we apply the method introduced in Sec. III of Paper I to obtain the corresponding radial scattering equations in the $\{L\Lambda S\Sigma\}$ representation. Because the derivation, with minor differences in details, is essentially unchanged from that given in Paper I, we stress only the highlights here. The interested reader is urged to follow the more detailed discussion given in Paper I. Following the procedure outlined by Eqs. (25)–(38) in Paper I, we obtain the scattering equations for the amplitudes $\underline{F}(\mathbf{R}) \equiv F_{L\Lambda S\Sigma}(\mathbf{R})$ in the $\{L\Lambda S\Sigma\}$ representation,

$$\frac{-1}{2\mu}(\underline{I}\nabla - i\underline{\mathbf{A}})^2 \underline{F}(\mathbf{R}) + \underline{V}(\mathbf{R})\underline{F}(\mathbf{R}) = E\underline{F}(\mathbf{R}) \ , \tag{14}$$

where $\underline{\mathbf{A}}$ is a vector potential [18], and $\underline{V}(\mathbf{R})$ is now given by

$$[\underline{V}(\mathbf{R})]^{L'\Lambda'S'\Sigma'}_{L\Lambda S\Sigma} = \delta^{L'\Lambda'S'\Sigma'}_{L\Lambda S\Sigma} \epsilon_{L\Lambda S}(R) \ . \tag{15}$$

Unlike the case in the $\{j\Omega j_a j_b\}$ representation, the molecular-gauge potential matrix $\underline{V}(\mathbf{R})$ is diagonal, and all transitions are induced by the off-diagonal elements of the vector potential $\underline{A}(\mathbf{R})$. Because the vector coupling $\underline{A}(\mathbf{R})$ persists in the $R \to \infty$ limit [6], we construct a unitary transformation (gauge transformation) and define a new amplitude $\underline{G}(\mathbf{R}) = \underline{T}(\theta\phi)\underline{F}(\mathbf{R})$, where $\underline{T}(\theta\phi)$ is a unitary matrix. In this representation we define

$$\begin{aligned}[\underline{T}(\theta\phi)]^{L\Lambda S\Sigma}_{L'\Lambda'S'\Sigma'} &\equiv \langle \Sigma S\Lambda L | \exp(-i\phi j_z) \exp(-i\theta j_y) \\ &\quad \times \exp(i\phi j_z) | L'\Lambda'S'\Sigma' \rangle \\ &= D^L_{\Lambda,\Lambda'}(\phi,\theta,-\phi) D^S_{\Sigma,\Sigma'}(\phi,\theta,-\phi) \\ &\quad \times \delta_{L,L'} \delta_{S,S'} \ ,\end{aligned} \tag{16}$$

where j_x, j_y, j_z are total electron angular-momentum operators [6],

$$D^l_{\Omega,\Omega'}(\phi,\theta,-\phi) \equiv \exp[-i\phi(\Omega-\Omega')] d^l_{\Omega,\Omega'}(\theta) \ , \tag{17}$$

and $d^l_{\Omega,\Omega'}(\theta)$ is a reduced Wigner function [19]. Carrying out the transformation we find that the amplitude $\underline{G}(\mathbf{R})$ obeys [20]

$$\frac{-1}{2\mu}\nabla^2 \underline{G}(\mathbf{R}) + [\underline{V}'(\mathbf{R}) - \underline{E}]\underline{G}(\mathbf{R}) = 0 \ , \tag{18}$$

where

$$\begin{aligned}[\underline{V}'(\mathbf{R})]^{L\Lambda S\Sigma}_{L'\Lambda'S'\Sigma'} &= \delta_{L,L'}\delta_{S,S'} \sum_{\Omega\Sigma_1} D^L_{\Lambda,\Omega}(\phi,\theta,-\phi) D^L_{\Omega,\Lambda'}(\phi,\theta,-\phi) D^S_{\Sigma,\Sigma_1}(\phi,\theta,-\phi) D^S_{\Sigma_1,\Sigma'}(\phi,\theta,-\phi) \epsilon_{\Omega SL}(R) \\ &= \delta_{L,L'}\delta_{S,S'}\delta_{\Sigma,\Sigma'} \sum_{\Omega} D^L_{\Lambda,\Omega}(\phi,\theta,-\phi) D^L_{\Omega,\Lambda'}(\phi,\theta,-\phi) \epsilon_{\Omega SL}(R)\end{aligned} \tag{19}$$

and we have ignored the transformed vector potential $\underline{A}'(\mathbf{R})$ and the nonadiabatic component of the scalar potential since it is proportional to $1/2\mu$. Expression (19) is the molecular generalization of the atom-atom interaction term given by Eq. (9) in the discussion of Allison and Burke [4].

We introduce the partial-wave expansion

$$G_{L\Lambda S\Sigma}(\mathbf{R})=\sum_{lm}\sum_{Qq}\begin{bmatrix} L & l & Q \\ \Lambda & m & -q \end{bmatrix} \times Y_{lm}(\theta\phi)[Q]^{1/2}\frac{G^{Qq}_{LlS\Sigma}(R)}{R} , \quad (20)$$

where $G^{Qq}_{LlS\Sigma}(R)$ is the Q,qth radial partial scattering amplitude, and repeating steps described by the discussion framed by Eqs. (67)–(74) in Paper I, we arrive at the radial equations

$$-\frac{1}{2\mu}\left[\frac{d^2}{dR^2}-\frac{l(l+1)}{R^2}\right]G^{Qq}_{LlS\Sigma}(R) + \sum_{L'l'S'\Sigma'} V^{LlS\Sigma}_{L'l'S'\Sigma'}(Q;R)G^{Qq}_{L'l'S'\Sigma'}(R)=EG^{Qq}_{LlS\Sigma}(R) , \quad (21)$$

where

$$V^{LlS\Sigma}_{L'l'S'\Sigma'}(Q;R)=\delta_{S,S'}\delta_{\Sigma,\Sigma'}\delta_{L,L'} \times\sum_{\Omega}[l,l']^{1/2}\begin{bmatrix} L & l & Q \\ \Omega & 0 & -\Omega \end{bmatrix} \times\begin{bmatrix} L & l' & Q \\ \Omega & 0 & -\Omega \end{bmatrix}\epsilon_{\Omega LS}(R) \quad (22)$$

is a radial multipole potential. Equation (21) is the analogue of radial equation (2) derived in the $\{jlj_aj_b\}$ representation. In this representation the radial potential is diagonal with respect to the atomic quantum numbers LS, and the numerical effort required to integrate the radial equations is greatly reduced. Instead of integrating 81 coupled equations, the LS representation allows simplification to sets of uncoupled equations involving only five, three, and single channels. The S matrix is constructed in this representation and the S matrix in the $\{jlj_aj_b\}$ representation may be gotten from it by a unitary similarity transformation. We describe this method below. A similar procedure was also exploited by Allison and Burke.

We use Eq. (22) to construct the radial S matrix, $[S(Q)]^{LlS\Sigma}_{L'l'S'\Sigma'}$ for the Qth partial wave, and the amplitude for the system to undergo a transition from an electronic state $L'\Lambda'S'\Sigma'$ to state $L\Lambda S\Sigma$ and for the nuclei to scatter into solid angle $d\theta\sin\theta\, d\phi$ following an initial approach along the incident wave vector $\mathbf{K}_i$ with polar angles $\theta_i\phi_i$ is expressed by the partial-wave expansion

$$f^{L'\Lambda'S'\Sigma'}_{L\Lambda S\Sigma}(\theta\phi;\theta_i\phi_i)=\sum_{lm}\sum_{l'm'}\sum_{Qq}\delta_{L,L'}\delta_{S,S'}\delta_{\Sigma,\Sigma'}\begin{bmatrix} L & l & Q \\ \Lambda & m & -q \end{bmatrix}\begin{bmatrix} L & l' & Q \\ \Lambda' & m' & -q \end{bmatrix} \times Y_{lm}(\theta\phi)Y^*_{l'm'}(\theta_i\phi_i)[Q]\frac{2\pi i}{\sqrt{2\mu E}}[\underline{I}-\underline{S}(Q)]^{L'l'S'\Sigma}_{LlS\Sigma} . \quad (23)$$

$f^{L'\Lambda'S'\Sigma'}_{L\Lambda S\Sigma}(\theta\phi;\theta_i\phi_i)$ is related to the scattering amplitude in the $\{j\Omega j_aj_b\}$ representation, given by Eq. (94) in Paper I, by the unitary similarity transformation

$$f^{j'\Omega'j'_aj'_b}_{j\Omega j_aj_b}(\theta\phi;\theta_i\phi_i)=\sum_{L\Lambda S\Sigma}\sum_{L'\Lambda'S'\Sigma'}W^{L\Lambda S\Sigma}_{j\Omega j_aj_b}f^{L'\Lambda'S'\Sigma'}_{L\Lambda S\Sigma}(\theta\phi;\theta_i\phi_i)W^{L'\Lambda'S'\Sigma'}_{j'\Omega'j'_aj'_b} . \quad (24)$$

Multiplying both sides of Eq. (24) with spherical harmonics whose arguments are the incident and observation angles, integrating and averaging over these angles, using definition (11) and relation (94) in Ref. [6], we derive the relation

$$[S(J)]^{j'l'j'_aj'_b}_{jlj_aj_b}=\sum_{Q}\sum_{LS}(-1)^{j+j'+l+l'}[Q,L,S][j,j',j_a,j_b,j'_a,j'_b]^{1/2} \times\begin{Bmatrix} S & J & Q \\ l & L & j \end{Bmatrix}\begin{Bmatrix} S & J & Q \\ l' & L & j' \end{Bmatrix}\begin{Bmatrix} 1 & 1 & j_a \\ 1 & 1 & j_b \\ L & S & j \end{Bmatrix}\begin{Bmatrix} 1 & 1 & j'_a \\ 1 & 1 & j'_b \\ L & S & j' \end{Bmatrix}[S(Q)]^{LlS\Sigma}_{LlS\Sigma} . \quad (25)$$

In this derivation we contracted products of 3-j symbols into 6-j symbols, and used $l_a=l_b=s_a=s_b=1$. Relationship (25) is a useful diagnostic tool and we employed it to check the integrity of the numerical procedure used to solve Eq. (2). For example, we solved Eq. (11) for the radial amplitude in the $\{L\Lambda S\Sigma\}$ representation and obtained the $\underline{S}(Q)$ matrix, for $Q=J+2,J+1,J,J-1$, and $J-2$, where $J=11$ and $E=0.0025$ a.u. The squares

$|[S(Q)]^{LI'S\Sigma}_{LIS\Sigma}|^2$ of the S-matrix elements are tabulated in Table II, and in Table III we tabulate the squares of the reduced S-matrix elements

$$|S(J)^{j_a'j_b'}_{j_aj_b}|^2 \equiv \sum_{jj'll'} |[S(J)]^{j'l'j_a'j_b'}_{jlj_aj_b}|^2$$

obtained by applying relation (25) to the calculated values for $[S(Q)]^{LI'S\Sigma}_{LIS\Sigma}$. The reduced matrix elements $|S(J)^{j_a'j_b'}_{j_aj_b}|^2$ calculated this way were compared to the values obtained when we solved Eq. (2), setting the fine-structure energy defects to zero, directly. The two methods gave identical results, within six significant figures, for the reduced S matrix (and hence the transition cross sections).

TABLE II. Square of the S matrix elements $|S^{LSl}_{LSl'}(Q)|^2$ for values of total angular momentum $Q=9$, 10, 11, 12, 13, obtained in the L-S representation.

S	L	l	l'	$Q=9$	$Q=10$	$Q=11$	$Q=12$	$Q=13$
0	0	Q	Q	1.000	1.000	1.000	1.000	1.000
0	1	$Q-1$	$Q-1$	0.295	0.249	0.202	0.154	0.109
0	1	$Q-1$	$Q+1$	0.705	0.751	0.798	0.846	0.891
0	1	Q	Q	1.000	1.000	1.000	1.000	1.000
0	1	$Q+1$	$Q+1$	0.295	0.249	0.202	0.154	0.109
0	2	$Q-2$	$Q-2$	0.433	0.460	0.485	0.510	0.534
0	2	$Q-2$	Q	0.166	0.129	0.096	0.066	0.041
0	2	$Q-2$	$Q+2$	0.401	0.411	0.419	0.424	0.425
0	2	$Q-1$	$Q-1$	0.095	0.137	0.193	0.262	0.344
0	2	$Q-1$	$Q+1$	0.905	0.863	0.807	0.738	0.656
0	2	Q	Q	0.726	0.786	0.845	0.900	0.945
0	2	Q	$Q+2$	0.108	0.085	0.059	0.034	0.014
0	2	$Q+1$	$Q+1$	0.095	0.137	0.193	0.262	0.344
0	2	$Q+2$	$Q+2$	0.491	0.504	0.522	0.541	0.560
1	0	Q	Q	1.000	1.000	1.000	1.000	1.000
1	1	$Q-1$	$Q-1$	0.802	0.753	0.695	0.628	0.552
1	1	$Q-1$	$Q+1$	0.198	0.247	0.305	0.372	0.448
1	1	Q	Q	1.000	1.000	1.000	1.000	1.000
1	1	$Q+1$	$Q+1$	0.802	0.753	0.695	0.628	0.552
1	2	$Q-2$	$Q-2$	0.645	0.666	0.687	0.707	0.726
1	2	$Q-2$	Q	0.020	0.009	0.002	0.000	0.006
1	2	$Q-2$	$Q+2$	0.335	0.325	0.311	0.292	0.268
1	2	$Q-1$	$Q-1$	0.827	0.778	0.718	0.649	0.571
1	2	$Q-1$	$Q+1$	0.173	0.222	0.282	0.351	0.429
1	2	Q	Q	0.941	0.976	0.997	0.996	0.968
1	2	Q	$Q+2$	0.039	0.015	0.001	0.003	0.026
1	2	$Q+1$	$Q+1$	0.827	0.778	0.718	0.649	0.571
1	2	$Q+2$	$Q+2$	0.625	0.660	0.688	0.705	0.706
2	0	Q	Q	1.000	1.000	1.000	1.000	1.000
2	1	$Q-1$	$Q-1$	0.447	0.428	0.408	0.385	0.362
2	1	$Q-1$	$Q+1$	0.553	0.572	0.592	0.615	0.638
2	1	Q	Q	1.000	1.000	1.000	1.000	1.000
2	1	$Q+1$	$Q+1$	0.447	0.428	0.408	0.385	0.362
2	2	$Q-2$	$Q-2$	0.477	0.479	0.475	0.463	0.444
2	2	$Q-2$	Q	0.389	0.362	0.337	0.311	0.287
2	2	$Q-2$	$Q+2$	0.133	0.158	0.189	0.226	0.269
2	2	$Q-1$	$Q-1$	0.008	0.003	0.001	0.002	0.008
2	2	$Q-1$	$Q+1$	0.992	0.997	0.999	0.998	0.992
2	2	Q	Q	0.324	0.340	0.357	0.376	0.397
2	2	Q	$Q+2$	0.287	0.298	0.307	0.313	0.317
2	2	$Q+1$	$Q+1$	0.008	0.003	0.001	0.002	0.008
2	2	$Q+2$	$Q+2$	0.580	0.544	0.505	0.461	0.414

V. RESULTS AND DISCUSSION

We integrated Eq. (2), using an implementation of the log-derivative algorithm of Johnson [21], to obtain the S matrix and Eq. (6) was used to construct the transition cross sections. The potential matrix (3) was constructed using tables of the $3j$ and $9j$ symbols which were calculated using an algorithm of Schulten and Gordon [22]. Some simplification in the system of 81 coupled channels is achieved by using parity conservation to reduce these equations into two independent sets, having dimensions $N=41$ and 40, respectively. We used an integration step size of about $0.01a_0$ and integrated the equations from $R=0$ to $R\approx 15a_0-20a_0$. With these values for the integration parameters we achieve an accuracy of about $0.001a_0^2$ for the inelastic transition cross sections, though at higher energies a smaller step size is required.

In order to explore the sensitivity of the calculated cross sections under various simplifying assumptions used in a previous calculation [4], we attempted to reproduce the results of Allison and Burke within our framework. We solved Eq. (2) in the hard-core-potential approximation [4] for $R<5a_0$, and replaced the Born-Oppenheimer potentials $\epsilon_{\Lambda SL}$ with the long-range form C_5/R^5 [4]. We also set the fine-structure energy defects in each atom to zero. The results of this calculation, for an energy corresponding to the wave number $k^2=2\mu E=96.0$ a.u., are given in Table IV and are labeled by σ_A. The values reported in Ref. [4], divided by a factor of 2 [23], are labeled σ_B. Our results are in good agreement with the ones given by Allison and Burke, with most cross sections agreeing to within 10%; the largest discrepancy, for $\sigma(22\rightarrow 01)$, is about 20%. We do not know why the cross sections are not in better agreement, except to note that Allison and Burke did not specify the exact value of the hard-core-potential cutoff point, and this may introduce some uncertainty in the comparison. We stress that our calculations were done in the $\{j\Omega j_aj_b\}$ representation, and so the general agreement with the previous calculation, done in the $\{L\Lambda S\Sigma\}$ representation, is another independent check of our numerical procedure. In the column labeled by σ_C we repeat the calculation, but now include accurate molecular potentials. Though Allison and Burke argued that molecular effects are unimportant in this energy region, our results clearly indicate that molecular effects are quite significant, altering some cross sections by more than a factor of 2. Finally, in the last column, labeled by σ_D, we present the cross sections obtained when the fine-structure energy defects are included. We found that inclusion of the fine-structure splitting alters most cross sections dramatically.

Table IV is divided into three groups of rows. The first group identifies the nine transitions in which one atom undergoes an elastic transition while the other atom

TABLE III. The square of the effective S-matrix elements $|S^{j'_a j'_b}_{j_a j_b}(J)|^2$ in the j-j representation for $J=11$.

$j_a j_b$ \ $j'_a j'_b$	00	01	10	02	20	12	21	22	11
00	0.000	0.000	0.000	0.000	0.000	0.000	0.000	0.000	0.000
01		2.064	0.043	0.054	0.033	0.364	0.437	0.423	0.384
10			2.064	0.033	0.054	0.437	0.364	0.423	0.384
02				2.734	0.032	0.229	0.885	0.578	0.062
20					2.734	0.885	0.229	0.578	0.062
12						10.67	1.068	2.746	0.817
21							10.67	2.746	0.817
22								15.07	1.269
11									4.542

makes an inelastic (endothermic) transition. The second group contains the five transitions where both atoms undergo an excitation transition. The third group denotes transitions where one atom undergoes excitation while the second atom makes an exothermic transition. We define a dimensionless parameter $y \equiv \Delta E / E_i$, where ΔE is the total energy difference of the internal states of both atoms after and before a collision, and E_i is the total kinetic energy in the entrance channel. For each transition the corresponding y parameter is tabulated, and looking at the Table IV we note a trend. Generally, smaller y translates into smaller differences between σ_D and σ_C. Transitions characterized by larger values of y have cross sections that are significantly smaller than those predicted by the degenerate-level model. The second group of transitions involving two-atom excitations have larger y values and Table IV shows that the corresponding cross sections are, sometimes, orders of magnitude smaller than the degenerate fine-structure level model predicts. A notable exception to this trend is the cross section $\sigma(20 \rightarrow 00)$ which corresponds to the transition where y has a large value (0.46) though σ_D and σ_C differ by only about 25%.

In Table V we tabulate the calculated cross sections $\sigma(j_a j_b \rightarrow j'_a j'_b)$ for collision energies in the range $0.0025 < E < 0.0070$ a.u. The table is divided into the

TABLE IV. Cross sections for fine-structure transitions using different approximations. All cross sections are calculated for a relative collision energy corresponding to the wave number $k^2 = 2\mu E = 96.0$ a.u. σ_A are calculated using the approximation outlined in Ref. [4], σ_B are cross sections, divided by a factor of 2, given in Ref. [4], σ_C are calculated using a molecular potential within the degenerate fine-structure approximation, and σ_D are the cross sections calculated using molecular potentials and accurate fine-structure splitting. The parameter y represents the ratio of the energy defect of the given transition to the value of the relative collision energy in the entrance channel. All cross sections are in units of a_0^2.

$j_a \rightarrow j'_a$	$j_b \rightarrow j'_b$	σ_A	σ_B	σ_C	y	σ_D
2→1	2→2	27.50	26.81	39.28	0.22	14.50
2→0	2→2	5.819	5.219	11.29	0.31	0.844
1→0	2→2	13.44	13.21	17.54	0.12	12.96
2→1	1→1	14.91	14.06	23.09	0.28	4.574
2→0	1→1	5.249	5.185	7.196	0.40	0.470
1→0	1→1	8.880	9.134	10.17	0.17	11.43
2→1	0→0	3.262	3.236	4.565	0.32	2.240
2→0	0→0	0.806	0.815	1.768	0.46	1.314
1→0	0→0	2.883	2.766	3.449	0.20	0.638
2→1	2→1	15.57	13.98	26.43	0.44	0.849
2→0	2→1	4.631	3.800	8.857	0.53	0.051
2→0	2→0	1.783	1.419	3.228	0.63	0.019
1→0	2→0	0.844	0.860	1.223	0.52	0.040
1→0	1→0	6.589	6.929	6.132	0.34	3.212
0→1	2→1	20.54	21.38	17.69	0.18	25.89

TABLE V. Cross sections for transitions from initial atomic oxygen fine-structure levels $j_a j_b$ into final levels $j'_a j'_b$. All cross sections are in units of a_0^2.

$j_a \rightarrow j'_a$	$j_b \rightarrow j'_b$	Energy (a.u.)				
		0.0025	0.004	0.005	0.006	0.007
2→1	2→2	6.927	15.47	16.92	18.53	12.52
2→0	2→2	0.458	1.051	1.338	1.604	1.424
1→0	2→2	7.836	14.48	14.10	13.91	9.165
2→1	1→1	1.937	5.608	7.012	8.538	6.723
2→0	1→1	0.082	0.710	1.063	1.370	1.104
1→0	1→1	3.258	12.14	11.44	10.74	6.993
2→1	0→0	1.010	2.264	2.575	3.003	2.344
2→0	0→0	1.192	1.524	1.744	1.717	1.543
1→0	0→0	0.258	0.868	1.116	1.338	1.562
2→1	2→1	1.082	1.092	1.475	1.822	1.806
2→0	2→1	0.079	0.087	0.150	0.215	0.234
2→0	2→0	0.003	0.038	0.065	0.096	0.124
1→0	2→0	0.030	0.060	0.101	0.144	0.170
1→0	1→0	2.855	3.838	4.879	5.607	5.870
0→1	2→1	15.89	24.29	22.38	20.78	13.49

three groups which identify transitions involving one-atom excitation, two-atom excitation, and one-atom excitation, other-atom deexcitation, respectively. The remaining inelastic cross section, not tabulated, can be calculated using the principle of detailed balance. In general, the one-atom excitation cross sections are significantly larger than those involving excitation transitions in both atoms. Most cross sections increase monotonically to a local maximum at a collision energy near 0.006 a.u. before decreasing at higher energies.

The accuracy of the cross sections presented in Table V is limited by uncertainties in the O_2 *ab initio* potential curves, though it is unlikely that these uncertainties reflect errors exceeding 20% in the tabulated cross sections. Additional approximations, such as setting the fine-structure defects to have a constant value given by their asymptotic values, are expected to be valid [24]. We also neglected the effects of the nonadiabatic vector-potential couplings [6] but in Paper I we show that these derivative coupling terms vanish in the separated-atom limit and, since they are proportional to the inverse of the reduced mass of the O_2 system, we suspect that they provide a small contribution to the total cross sections at the collision energies of interest.

ACKNOWLEDGMENTS

This work has been supported by the AFOSR under the special initiative for thermospheric oxygen with funds administered by Task No. 2303EP and Phillips Laboratory Project No. 007, and by the National Science Foundation, Division of Atmospheric Sciences under Grant No. 93-20175. We thank the National Supercomputer Center for the Environment and Energy (NSCEE) for use of their supercomputer.

[1] D. R. Bates, Proc. Phys. Soc. London Sect. B **64**, 805 (1951).
[2] C. F. Fischer and H. P. Saha, Phys. Rev. A **28**, 3169 (1983).
[3] R. D. Sharma, H. B. Harlow, and J. P. Riehl, Planet. Space Sci. **36**, 531 (1988); R. D. Sharma, A. S. Zachor, and B. K. Yap, *ibid.* **38**, 221 (1990).
[4] D. C. Allison and P. G. Burke, J. Phys. B **2**, 941 (1969).
[5] K. U. Grossmann and D. Offermann, Nature **276**, 594 (1978).
[6] B. Zygelman, A. Dalgarno, and R. D. Sharma, Phys. Rev. A **49**, 2587 (1994).
[7] We note and correct a few typographical misprints in Ref. [6]. In that paper, the subscript θ should be replaced with ϕ on the third and fourth lines of Eq. (55). In Eq. (78) $G(\mathbf{R})$ should be replaced with $G_\gamma(\mathbf{R})$, and the reference, on the second sentence of page 2600, to Eq. (26) should be replaced by a reference to Eq. (25).
[8] Care must be taken when defining the total electronic angular momentum; see Ref. [6].
[9] The scattering matrix is independent of the azimuthal quantum number [6] and so we use a notation where the dependence on M is implicit, e.g., $S(JM) \equiv S(J)$, etc.
[10] B. Liu and R. Saxon, J. Chem. Phys. **67**, 5432 (1977).
[11] H. Partridge, C. W. Bauschlinger, Jr., Stephen R. Langhoff, and P. R. Taylor, J. Chem. Phys. **95**, 8292 (1991).
[12] The $C^3\Delta_u$ state is alternatively designated as the $A'^3\Delta_u$ state in Ref. [11].
[13] J. K. Knipp, Phys. Rev. **53**, 734 (1939).
[14] T. Y. Chang, Rev. Mod. Phys. **39**, 911 (1967).
[15] S. J. A. Uminskij and E. E. Nikitin, Theor. Chem. Acta **13**, 91 (1969).
[16] In Ref. [6] we expressed the C_5 coefficients in units of $\langle r^2 \rangle^2/25$, where $\langle r^2 \rangle$ is the radial expectation value of the atomic oxygen electrons. Using the calculated value $\langle r^2 \rangle = 1.97$ [E. Clementi, J. Chem. Phys. **41**, 303 (1964)] we obtain the values tabulated in Table I.
[17] D. C. Allison, P. G. Burke, and W. D. Robb, J. Phys. B **5**, 1431 (1972).
[18] In the $\{L\Lambda S\Sigma\}$ representation the vector potential $\underline{A}$ is given by a similarity transformation of expression (41) in Ref. [6].
[19] R. N. Zare, *Angular Momentum* (Wiley, New York, 1988).
[20] We neglect the transformed nonadiabatic vector and scalar potentials. See the discussion in Ref. [6] regarding the validity of this approximation.
[21] B. R. Johnson, J. Comput. Phys. **13**, 445 (1973).
[22] K. Schulten and R. G. Gordon, J. Math. Phys. **16**, 1961 (1975).
[23] The cross sections defined by Eq. (21) of Ref. [4] are properly symmetrized but do not include an extra factor of $\frac{1}{2}$ that results when the flux of the incident symmetrized wave function is normalized to unity [6].
[24] C. N. Challacombe and G. M. Almy, Phys. Rev. **51**, 930 (1937).